Synthesis and characterisation of substituted diphenylamines—charge-transfer, donor–acceptor systems localised at water–oil interfaces†

K. Kowalski,[ab] N. J. Long,*[a] M. K. Kuimova,[a] A. A. Kornyshev,[a] A. G. Taylor[a] and A. J. P. White[a]

Received (in Durham, UK) 15th October 2008, Accepted 20th November 2008
First published as an Advance Article on the web 15th December 2008
DOI: 10.1039/b818110a

A range of charge-transfer, donor–acceptor systems have been synthesised and subjected to in-depth crystallographic, spectroscopic and interfacial studies. The pyridine- or phenyl-substituted (*N*,*N*-diphenyl)amino derivatives contain an identical donor unit, NR_3, and acceptor species with varying acceptor strength, with three compounds (**3**, **6** and **9**) being characterised by X-ray structural analysis. Two of the compounds, the methyl **6** and octyl **8** derivatives, show interfacial localisation *via* fluorescence confocal microscopy and illustrate their potential as light-driven optical machines.

Introduction

The chemistry and physics of liquid–liquid interfaces is an increasingly important area of interdisciplinary research. Many fundamental processes in nature and technology take place at liquid interfaces *e.g.* uptake and reactions of pollutants at the surface of water droplets and ice particles in the atmosphere, phase transfer catalysis and ion-, electron- and proton-transfer reactions at liquid–liquid and liquid–membrane interfaces.[1–3] Such interfaces are also ideal candidates for the assembly of functional supramolecular architectures, with potential supply of building blocks dissolved in either of the liquid phases. One very promising system is the interface of two immiscible electrolytic solutions (ITIES), a solution of organic ions in oil and inorganic ions in water that has a large free energy of transfer between the two liquids.[4] Following an application of an external electric field, two 'back-to-back' electrical double layers are formed on each side of the liquid–liquid interface. Thus created voltage drops, up to 0.5 V $Å^{-1}$,[5] can offer an additional degree of control of supramolecular assembly and its functions. Current interest in ITIES stems from the fact that it could be used as a medium for phase transfer catalysis,[6] an environment for artificial photosynthesis and solar energy conversion.[7]

Since ITIES are accessible for self-assembly processes from both phases, they constitute a very promising environment for the self-assembly of interfacial supramolecular nano-scale objects with amphiphilic compartments.[8] Our goal is to design and synthesise a series of molecules with promising charge-transfer, donor–acceptor properties, which could localise at ITIES and be suitable to act as the light-driven molecular machines.

Donor–acceptor systems with large dipole moments have already found successful applications in non-linear optics,[9] solar energy conversion[10] and molecular electronics. The donor and acceptor moieties can be chosen such that the highest lying molecular orbital (HOMO) is localised on the donor part and the lowest unoccupied molecular orbital (LUMO) on the acceptor part. Thus a transition from HOMO to LUMO following excitation results in the formation of the intramolecular charge-transfer (ICT) excited state. The particular strength of this approach is that the energy of the ICT transitions can be finely tuned by chemical modifications which affect the redox potential of either the donor or acceptor parts.

For an efficient utilisation of the excitation energy it is important to have the maximum overlap between the absorption spectrum of the molecule and the light source. For example, for the solar energy conversion the overlap with the solar spectrum, *ca.* 400–500 nm maximum, is required. For non-linear optical applications, such as second harmonic generation (SHG), the spectral overlap with the output of the commercially available pulsed lasers is desirable. Widely commercially available Ti:sapphire femtosecond lasers have the emission maximum of *ca.* 800 nm, indicating that for resonance enhancement of SHG the absorption at *ca.* 400 nm might be beneficial.

In the course of this project a theory was developed[11] that describes the operation of such machines, termed 'optical teaspoons', that encompasses the modes of conformational motion of the molecule depending on different initial orientation and charge distribution, as well as various applied voltages. That treatment describes the anticipated optical response to the application of an external electric field, on both steady state and time resolved properties of the interfacial chromophore (electrochromic effects). In parallel we carried

[a] *Department of Chemistry, Imperial College London, South Kensington, London, UK SW7 2AZ*
[b] *Department of Organic Chemistry, Faculty of Chemistry, University of Łódź, Narutowicza 68, 90-136 Łódź, Poland*

† Electronic supplementary information (ESI) available: Details of crystallographic refinements, thermal ellipsoid plots and CIF files. CCDC reference numbers 696198–696200. For ESI and crystallographic data in CIF or other electronic format see DOI: 10.1039/b818110a

out the synthesis of the candidate molecules, which could be exploited as 'optical teaspoons', thus in this manuscript we report the synthesis of a series of compounds, **1–10**, all of which contain an identical donor moiety, NR_3, and acceptor moieties with varying acceptor strengths. The primary goal of the present publication was to ascertain that our target molecules (i) localise at the water–oil interface, suitable for the formation of ITIES, (ii) possess desirable charge-transfer properties and (iii) show the spectral overlap with the tuning curve of the Ti:sapphire femtosecond laser, to enable future SHG studies.

Synthesis and spectroscopic characterisation

In the synthesis of the candidate molecules, the compounds were designed to possess clear hydrophobic and hydrophilic functionalities to enable interfacial localisation. Pyridine or phenyl-substituted (*N*,*N*-diphenyl)amino derivatives were focussed on due to their ease of synthesis, rod-like structures, low cost, photochemical and SHG properties. For example, 2-(*N*-methyl-*N*-isopropylamino)-5-cyanopyridine exhibits so-called twisted internal charge-transfer (TICT),[12] molecules of (*N*,*N*-di-*p*-tolylamino-*p*-styryl)benzene can self-organise on surfaces to form microdots,[13] tetraaryl amines exhibit SHG properties[14] and oligomeric and polymeric materials based on triphenylamine[15–17] can be electroluminescent and electron conductors. The synthetic strategy for compounds **1–5** was based on palladium-catalysed Suzuki coupling and is illustrated in Scheme 1.

Compounds **1–5** were isolated in high yields (*ca.* 80%) and easily purified *via* column chromatography. The structures and purity of **1–5** were confirmed by spectroscopic analysis (^{1}H, ^{13}C, MS, IR) and CHN microanalysis. For example, the ^{1}H NMR of **3** shows characteristic doublets for the nitro-substituted phenyl ring protons at 8.26 ppm and 7.69 ppm. A signal for the second disubstituted phenyl ring protons is present at 7.50 ppm. The remaining protons of the mono-substituted and disubstituted phenyl rings give two multiplets at 7.06–7.16 and 7.27–7.32 ppm, respectively. The high-resolution mass spectrum (HRMS, EI, 70 eV) of **3** shows a mass peak at 366.1368 *m*/*z* with the calculated value for $C_{24}H_{18}N_2O_2$ being 366.1368. Slow diffusion of *n*-hexane to a saturated CH_2Cl_2 solution of **3** afforded red-orange monocrystals suitable for X-ray analysis. The molecular

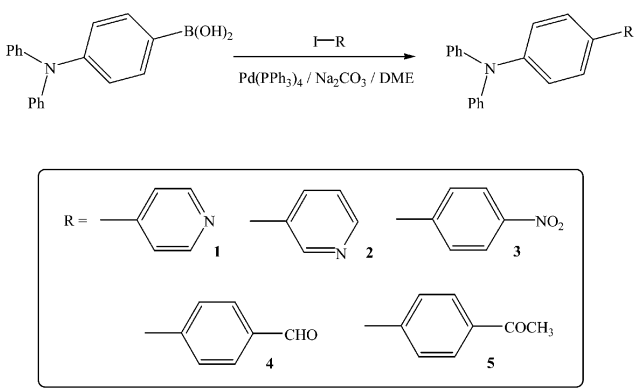

Scheme 1 Formation of compounds **1–5**.

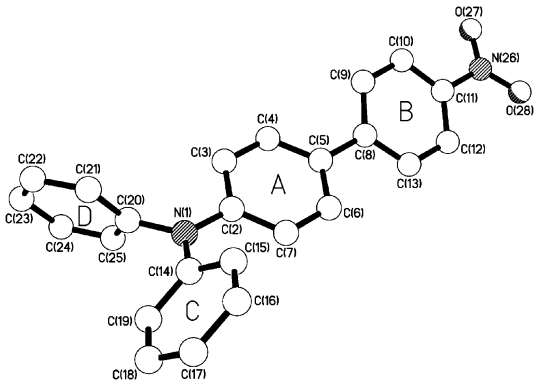

Fig. 1 The molecular structure of **3**.

structure of **3** is shown in Fig. 1 and reveals a series of twists along the N–Ar–Ar–NO_2 axis with torsion angles of *ca.* +22, +24 and −14 about the N(1)–**A**, **A**–**B** and **B**–NO_2 bonds, respectively, suggesting less than perfect alignment (and thus conjugation) of the π systems. Adjacent molecules stack to form a centrosymmetric "dimer pair" held together by N(π)···π and π–π contacts (interactions **a** and **b** in Fig. 2 here, and Fig. S2, ESI†). The N(π)···π interaction involves ring A in one molecule and the NO_2 group in a C_i-related counterpart, and has an N···centroid separation of *ca.* 3.72 Å [though the O(28) atom is closer to ring **A** centroid at *ca.* 3.49 Å]. The π–π interaction **b** between ring B and its centrosymmetrically related counterpart has centroid···centroid and mean inter-planar separations of *ca.* 3.73 and 3.60 Å, respectively, and the two rings are perfectly parallel due to them being C_i-related. Adjacent "dimer pairs" are held together by a C–H···π interaction between the C(23) proton on ring **D** in one dimer, and the "unused" face of ring **B** in another dimer (interaction **c** in Fig. 2 and S2, ESI†), resulting in an extended 2D sheet of dimers arranged in a parquet-like fashion (Fig. 2). The C–H···π interaction **c** has H···π 2.90 Å, C–H···π 122°, with the H···π vector being inclined by *ca.* 79° to the aromatic ring plane; the centroid···centroid and H···π vectors of interactions **b** and **c**, respectively, subtend an angle of *ca.* 157° at the ring **B** centroid.

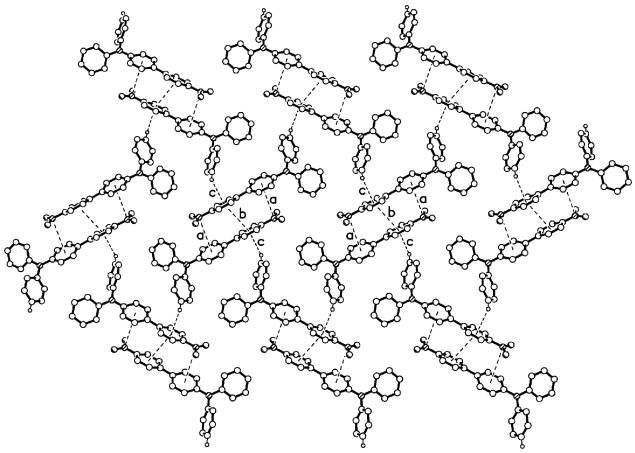

Fig. 2 Part of one of the 2D parquet-like sheets of C_i-related pairs of molecules present in the structure of **3**.

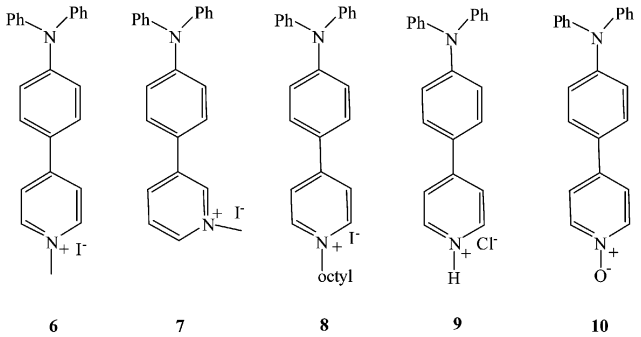

Scheme 2 Formation of compounds **6–10**.

Compounds **1–5** were then derivatised to include enough amphiphilic character to localise them onto a water–organic interface. This was executed *via* addition of carbon chains to the structure, protonation or oxidation of the pyridine nitrogen atom to form compounds **6–10**. For example, reaction of **1** with methyl iodide at room temperature afforded the *N*-methyl iodide salt **6** in good yields, as did the similar reaction of **2** to form **7** (Scheme 2). **1** was reacted with 1-iodooctane overnight at 70 °C to yield the long chain derivative **8** and the hydrochloride salt **9** was obtained *via* direct acidification of **1** *via* concentrated HCl addition. The *N*-oxide **10** was obtained by oxidation of **1** with 3-chloroperoxo benzoic acid (MCPBA).

The structures of compounds **6**, **7**, **8** and **10** were confirmed by spectroscopic analysis (^{1}H, ^{13}C, MS, IR) and microanalysis. Structural X-ray analysis was obtained for compounds **6** and **9**, though good microanalysis of **9** could not be obtained due to the relatively high amount of water present in the crystal lattice as confirmed by the X-ray analysis. The ^{1}H NMR spectrum of **6** shows 2H doublets for the pyridine ring at 9.07 ppm and 8.08 ppm, and 2H doublets for the C_6H_4 ring protons at 7.65 ppm and 7.03 ppm. A multiplet for the *ortho*-protons of the C_6H_5 ring is observed at 7.34–7.31 ppm and for the *meta*-, *para*-C_6H_5 ring protons it is at 7.18–7.13 ppm. The methyl group gives rise to a signal at 4.53 ppm. In the ^{13}C NMR spectrum, the diagnostic signal for the methyl group carbon is at 47.94 ppm. The mass spectrum (FAB^{+}) of **6** shows a mass peak for the cationic fragment at 337 *m*/*z* confirming the molecular ion. Slow diffusion of *n*-pentane into a saturated CH_2Cl_2 solution of **6** afforded deep-orange monocrystals suitable for X-ray analysis and the molecular structure of **6** is shown in Fig. 3. The structure was found to be highly disordered, with two 50% occupancy orientations (**I** and **II**) for the whole of the cation being identified (in fact, the iodine anion is the only ordered atom present)—see the ESI† for more details. Orientation **I** is shown in Fig. 3, orientation **II** in Fig. S4 (ESI†), and an overlay of both in Fig. S6 (ESI†). As a result of this extensive disorder neither the individual molecular or extended structures can be discussed in detail, but some broad features are worthy of mention. As was seen in the structure of 3, here for both orientations the N–Ar–Ar axis is twisted, and the packing is dominated by a stack of molecules in an alternating –**I**–**II**–**I**–**II**– fashion (Fig. 4, see the ESI† for why the stack has to be alternating). The centroid···centroid separations for the π–π interactions that form this stack are *ca.* 3.8 Å.

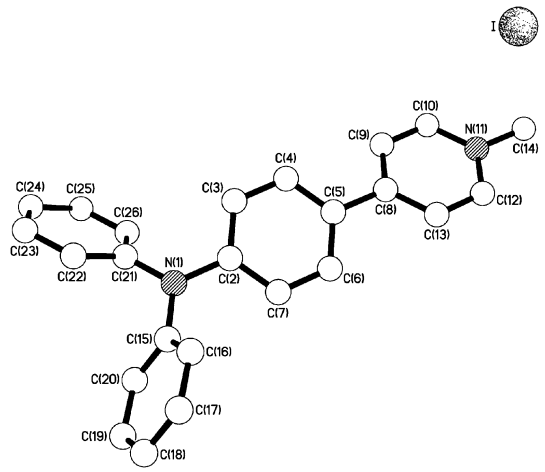

Fig. 3 The molecular structure of one (**6-I**) of the two 50% occupancy orientations present in the asymmetric unit of **6**.

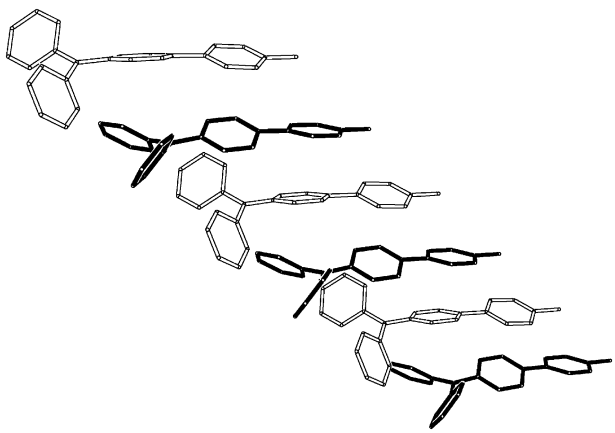

Fig. 4 Part of one of the alternating stacks of molecules present in the asymmetric unit of **6** (orientation **I** has been drawn with dark bonds, and **II** with open bonds).

The ^{1}H NMR spectrum of **7** shows signals for the pyridine protons at 9.32 ppm (1H singlet), 9.03 ppm (1H doublet), 8.47 ppm (1H doublet), 8.03 ppm (1H doublet of doublets). A doublet for the C_6H_4 ring protons is observed at 7.68 ppm and all the other aromatic proton signals give multiplets at 7.33–7.25 ppm (*ortho*-C_6H_5 protons) and 7.15–7.07 ppm (*meta*-, *para*-C_6H_5 and C_6H_4 protons). A singlet for the methyl group is observed at 4.74 ppm. The mass spectrum (FAB+) of **7** shows a mass peak of the cation fragment at 337 *m*/*z* confirming the presence of the molecular ion. The ^{1}H NMR spectrum of **8** shows doublets for the pyridine ring at 9.11 ppm and 8.10 ppm, and doublets for C_6H_4 ring protons at 7.66 ppm and 7.05 ppm. Multiplets for the *ortho*-protons of the C_6H_5 ring are observed at 7.37–7.33 ppm and for the *meta*-, *para*-C_6H_5 ring protons at 7.18–7.15 ppm. The signal at 4.75 ppm can be assigned to the two protons of the methylene group attached to the pyridine nitrogen, the remaining protons of the carbon chain give multiplets at 2.04–1.96 ppm and 1.41–1.16 ppm, and there is a three proton triplet for terminal methyl group protons at 0.84 ppm. The mass spectrum (FAB+) of **8** shows a mass peak of the cation fragment at 435 *m*/*z*.

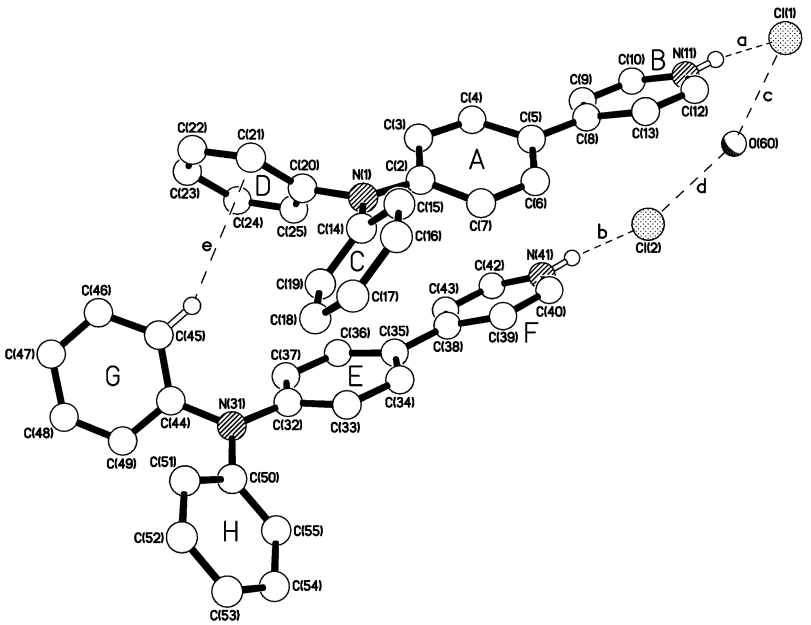

Fig. 5 The molecular structure of **9**. The geometries of the N–H···Cl hydrogen bonds [N···Cl] Å, [H···Cl] Å and [N–H···Cl]° are (**a**) 3.041(3), 2.15, 170, and (**b**) 3.040(2), 2.14, 173. The hydrogen bonds **c** and **d** have O···Cl separations of 3.249(4) and 3.261(3) Å, respectively. The C–H···π interaction **e** has H···π 2.90 Å, C–H···π 145°, with the H···π vector being inclined by *ca.* 81° to the aromatic ring plane.

The ^{1}H NMR spectrum of **10** shows a doublet for C_5H_4NO ring protons at 8.20 ppm, whilst all the other signals are grouped into three multiplets at 7.46–7.43 ppm (C_5H_4NO and C_6H_4 protons), 7.31–7.27 (*ortho*-C_6H_5 protons) and 7.14–7.07 (*meta*-, *para*-C_6H_5 and C_6H_4 protons). The high-resolution mass spectrum (HRMS, EI, 70 eV) of **10** shows a mass peak at 338.1417 m/z with the calculated value of $C_{23}H_{18}N_2O$ being 338.1419. Attempts to obtain a good quality ^{1}H NMR spectrum of **9** failed due to our assumption that in solution **9** is in equilibrium with nonprotonated **1**, and such fast proton exchange limited clear assignation of the signals. However by slow diffusion of *n*-pentane into a saturated CH_2Cl_2 solution of **9**, monocrystals suitable for X-ray analysis were obtained. The molecular structure of **9** is shown in Fig. 5 and revealed the presence of two crystallographically independent cation–anion pairs in the asymmetric unit, along with one water molecule and a highly disordered 50% occupancy dichloromethane molecule (the latter has been omitted from Fig. 5). Both independent cations show twists along their N–Ar–Ar axis with torsion angles of *ca.* +17 and −28 about the N(1)–**A** and **A**–**B** bonds, respectively, and *ca.* −27 and −11 about the N(31)–**E** and **E**–**F** bonds, respectively. Each chloride anion is linked to one of the cations by an N–H···Cl hydrogen bond (interactions **a** and **b** in Fig. 5), and to each other *via* the cocrystallised water molecule (interactions **c** and **d**). The N–H···Cl hydrogen bonds have [N···Cl] and [H···Cl] separations (Å), and [N–H···Cl] angles (°) of 3.041(3), 2.15, 170, and 3.040(2), 2.14, 173 for **a** and **b**, respectively. The O···Cl hydrogen bonds **c** and **d** have heteroatom separations of 3.249(4) and 3.261(3) Å, respectively (the water protons could not be located—see the ESI† for more details). The two cations are further linked by a C–H···π hydrogen bond between the C(45) proton and ring **D** (interaction **e**) with an H···π distance of *ca.* 2.90 Å, a C–H···π angle of *ca.* 145°, and with the H···π vector being inclined by *ca.* 81° to the ring plane. There is also a much weaker C–H···π interaction between the C(25) proton and ring **E** (not shown in the picture) with H···π 3.27 Å, C–H···π 115°, and the H···π vector inclined by *ca.* 60° to the ring plane. Both of the chloride anions sit above the centroids of pyridyl rings. As can be seen from Fig. 5, Cl(2) approaches the centroid of ring **B** with a Cl···centroid separation of *ca.* 3.95 Å (Cl···centroid vector inclined by *ca.* 64° to the ring plane), whilst Cl(1) is only *ca.* 3.98 Å from the centroid of ring **F** of a lattice translated cation (Cl···centroid vector inclined by *ca.* 59° to the ring plane).

There are numerous other intermolecular interactions in this structure that serve to link the unit shown in Fig. 5 to form a complex 3D array. The centroid of ring **A** is approached by the C(49) proton of a lattice translated unit with H···π 3.01 Å, C–H···π 135°, and the H···π vector inclined by *ca.* 63° to the ring plane. Ring **B** is involved in a π–π stacking interaction with ring **E** of a likewise lattice translated unit with centroid···centroid and mean interplanar separations of *ca.* 3.91 and 3.48 Å, respectively, the two rings being inclined by *ca.* 6° (the **E**···**B** centroid···centroid vector and the **B**···Cl(2) vector subtend an angle of *ca.* 177° at the ring **B** centroid). Ring **C** is approached by the C(46) proton from a C_i-related unit with H···π 3.05 Å, C–H···π 136°, and the H···π vector inclined by *ca.* 84° to the ring plane. The "unused" face of ring **D** is involved in a second C–H···π interaction, here with the C(45) proton from a lattice translated unit with H···π 2.92 Å, C–H···π 141°, and the H···π vector inclined by *ca.* 78° to the ring plane; the two interactions subtend an angle of *ca.* 160° at the ring **D** centroid. Both faces of ring **G** act as acceptors of C–H hydrogen bonds, from the C(53) and C(21) protons of lattice translated and C_i-related units, respectively, C(53)–H···**G** has H···π 2.91 Å,

C–H···π 150°, H···π vector inclined by *ca.* 76° to the ring plane; C(21)–H···**G** has H···π 3.21 Å, C–H···π 155°, H···π vector inclined by *ca.* 54° to the ring plane; the two interactions subtend an angle of *ca.* 131° at the ring **G** centroid. A similar pattern is seen for ring **H**, with approaches from the C(15) and C(24) protons of different lattice translated units—C(15)–H···**H** has H···π 2.83 Å, C–H···π 147°, H···π vector inclined by *ca.* 82° to the ring plane; C(24)–H···**H** has H···π 2.90 Å, C–H···π 151°, H···π vector inclined by *ca.* 73° to the ring plane; the two interactions subtend an angle of *ca.* 156° at the ring **H** centroid.

Physical characterisation and interfacial studies

Compounds **1–10** contain an identical donor moiety, NR_3, and acceptor moieties with varying acceptor strength. These compounds are analogous to donor–acceptor systems[9] in which the lowest excited state has been previously identified as ICT and these molecules have been shown by Hyper Rayleigh scattering with 800 or 1300 nm femtosecond pulses to possess high static first hyperpolarisabilities corresponding to high non-linear optical properties.[9]

Compounds **1–5** incorporate weak acceptor groups (high lying LUMOs), resulting in the high energy of the ICT transition, centred at *ca.* 350 nm. Compound **3** has additional strong bands associated with π–π* NO_2 group transitions at *ca.* 400 nm. Compounds **6–9** incorporate a stronger acceptor—the pyridinium group—which should result in the lower lying ICT states. Consistent with this, we observe the marked red shift of the lowest lying absorption maxima of **6**, **8** and **9** to *ca.* 420 nm (Table 1) indicating the significant lowering of the excited state energy. Surprisingly, compound **7** is characterised by an absorption maximum of 350 nm, similar to **1**, even though it has acceptor moiety similar to **6**. This could result from a different charge distribution pattern in **6** and **7**.

Following excitation into the lowest absorption band, emission is observed for **1**, **2**, **4–9** in several organic solvents and in water. The emission maximum is significantly red-shifted compared to the absorption maximum (the large Stokes shift), confirming the ICT nature of the lowest excited state. In addition the emission maxima of **6**, **8**, **9** are shifted to lower energy compared to **1**, consistent with lower lying LUMO (Fig. 6b). Absorption and emission maxima of **6**, **8**, **9** change as a function of solvent, *e.g.* see Fig. 7 for **6**. In conclusion, in the present series of compounds the absorption spectra of **6**, **8**, **9** represent the best match for the solar

Table 1 Absorption and emission properties of **1**, **6**, **8**, **9** in different solvents

	λ_{max}/nm (abs)/(emis)			
Solvent	**1**	**6**	**8**	**9**
Methanol	345/455	425/645	423/640	425/645
CH_2Cl_2	350/460	456/640	460/640	460/645
Toluene	345/460	427/470[a]	425/466[a]	425/—[b]

[a] The small Stokes shifts and the presence of a well defined vibrational structure in the emission spectra of **6** and **8** in toluene suggest that the emitting state is not ICT. [b] Not measured.

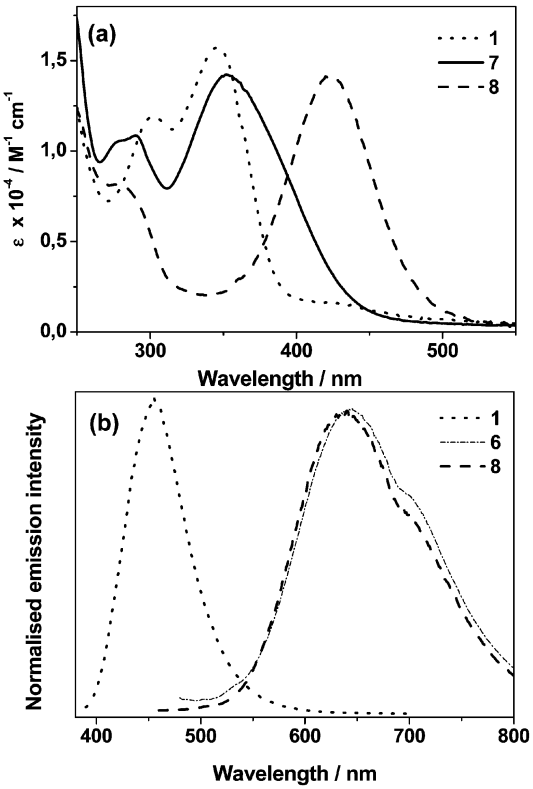

Fig. 6 (a) Absorption spectra of **1**, **7** and **8** and (b) emission spectra of **1**, **6** and **8** in methanol.

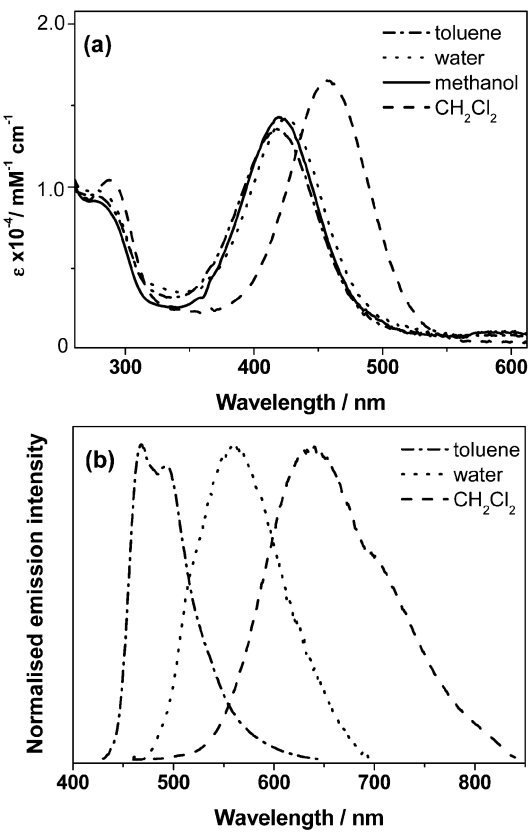

Fig. 7 (a) Absorption and (b) emission spectra of **6** in different solvents.

spectrum and for the output of the ultrafast Ti:sapphire lasers. In addition, there is the possibility to tune absorption and emission energy of these compounds with the environmental parameters.

Our target applications such as molecular electronics and SHG generation can benefit from *selective localisation* of a probe on the interface. Due to the preferential orientation of the probe, a much higher degree of order in the interfacial region could be achieved, resulting in a large cooperative dipole moment. The preferential localisation on the interface of the condensed/air phases is normally achieved by standard methods such as coating of the solid–air interface or Langmuir Blodgett film formation on the liquid–air interface. However these methods require deposition techniques to be used. An alternative solution is the spontaneous formation of the self-organised monolayers of the probe on the interface of two immiscible liquids. Compounds **6–9** consist of a large hydrophobic moiety with a single positive charge localised on one end. This charge renders compounds **6–9** water soluble and could assist in self-assembly on the liquid–liquid interface. Here we have directly tested the possibility of spontaneous formation of monolayers of **6**, **8** and **9** on water–oil interfaces using three complementary observations: (i) of surface tension in the interfacial region, (ii) of the bulk absorption change upon formation of the oil–water interface and (iii) of interfacial fluorophore localisation using confocal fluorescence microscopy.

The photographs of unmodified water–CH_2Cl_2 and water–toluene interfaces and interfaces in the presence of **6** and **8** (Fig. 8) clearly show the reduction in surface tension between the two immiscible liquids in the presence of **6** and **8**. The interfacial tension of oil *vs.* water is >30[18] as indicated by the curvature of the unmodified interface. Surfactants localised at the interface reduce the surface tension, causing the reduction in contact angle. A large reduction in contact angle is observed for **6** and **8**, indicating that these molecules are acting as surfactants and are preferentially localised on the water–oil interface.

To estimate the interfacial concentration of **6**, **8** and **9** we have used the change in absorption of either the aqueous or the oil layer containing the known concentration of these probes upon addition of the second layer. For example, the initial absorption of **6** in CH_2Cl_2 stock solution is *ca.* 0.05 ($\varepsilon = 1.8 \times 10^4$ M^{-1} cm^{-1} in CH_2Cl_2 and 1.4×10^4 M^{-1} cm^{-1} in water), which is equivalent to the concentration of 2.8 μM

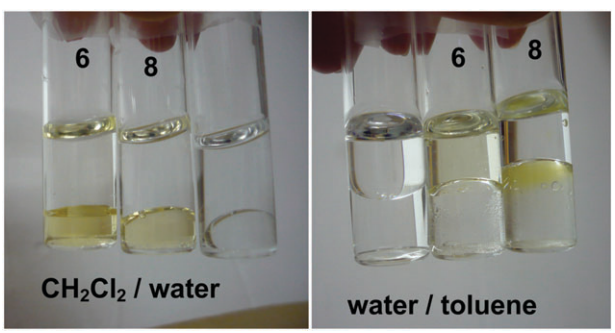

Fig. 8 Photographs of unmodified and modified interfaces.

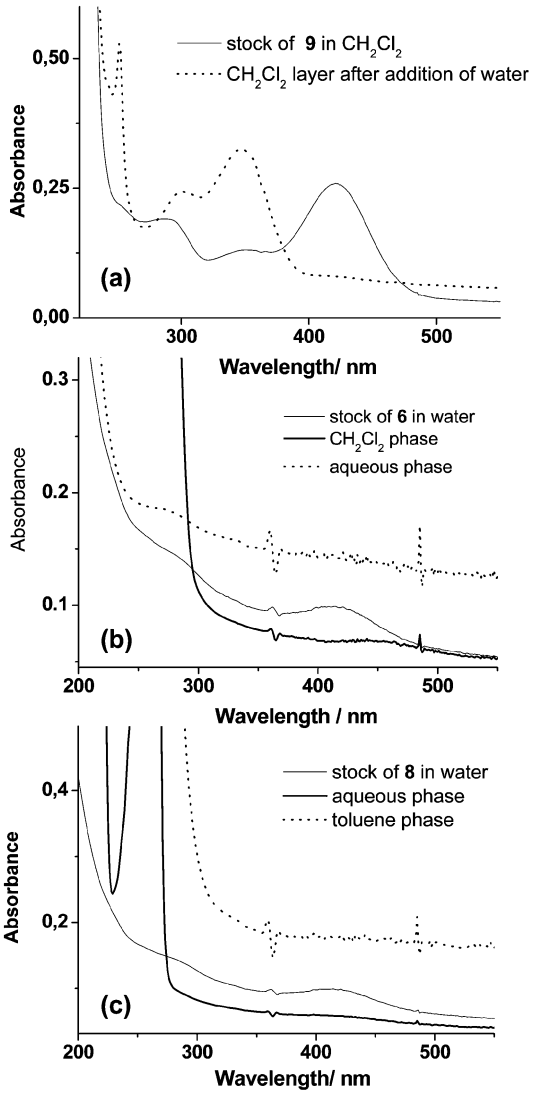

Fig. 9 Absorption study of interfacial concentration of **9** (a), **6** (b) and **8** (c). The change in absorption spectrum of **9** in CH_2Cl_2 upon addition of the aqueous layer is consistent with deprotonation. For **6** and **8** given the extinction coefficient of 1.8×10^4 M^{-1} cm^{-1} in CH_2Cl_2 and 1.4×10^4 M^{-1} cm^{-1} in water, we estimate from absorption change of *ca.* 0.05 OD that *ca.* 1e[15] molecules cm^{-2} are localised at the interface.

(in 0.5 ml). Upon addition of the second aqueous layer the resulting absorption of both CH_2Cl_2 and water layers is close to zero (Fig. 9b and c). The calculation shows that $\{(2.8 \times 10^{-6}$ M) $\times$ $(5 \times 10^{-4}$ l) $\times$ $(6.03 \times 10^{23}$ $mol^{-1})\}$/ 1 cm^2 $= 8 \times 10^{14}$ molecules cm^{-2} are localised on the liquid–liquid interface. For all the systems studied we obtain the interfacial concentration in the order 1×10^{15} molecules cm^{-2}.

Contrary to the observations for **6** and **8**, the surface tension of the water–oil interface does not change in the presence of **9**. In addition, the absorption spectroscopic study shows that upon addition of aqueous layer to the CH_2Cl_2 stock solution containing **9**, the absorption spectrum changes (Fig. 9a). The change from 420 nm absorption maximum to 350 nm maximum is consistent with deprotonation of **9** yielding compound **1** in the CH_2Cl_2 phase and protons in aqueous

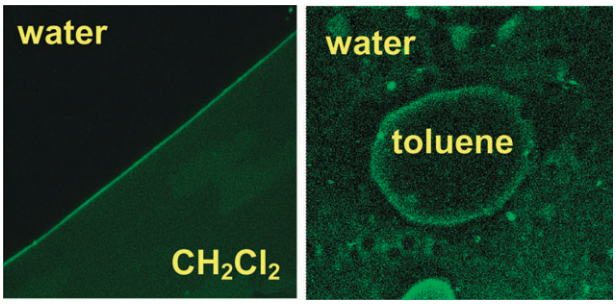

Fig. 10 Confocal fluorescence images of water–oil interfaces modified with **6** (water–CH_2Cl_2) and **8** (water–toluene).

phase, see Fig. 9a. Thus **9** is not sufficiently stable in the presence of water and is not suitable for formation of self-organised monolayers at aqueous–oil interface.

Additional confirmation of the interfacial localisation of **6** and **8** comes from the confocal fluorescence microscopy study (Fig. 10). The images of the interfacial region between water and oil phases obtained following 488 nm excitation clearly show intense fluorescence originating from the interfacial layer. The intensity of the fluorescence from the interfacial region is considerably higher than that observed from either of the bulk phases.

Conclusions and future work

In summary, we have synthesised a range of molecules with desirable charge-transfer properties that can localise on the ITIES and bear capability of light induced intramolecular electron transfer. We have performed a series of absorption measurements for a number of immiscible solvent combinations to determine which molecules and solvent systems would best fit their application in future light-driven molecular machines, such as 'interfacial optical teaspoons'.[11] These studies yielded two candidates that show interfacial localisation in water–toluene and water–dichloroethane mixtures—the methyl **6** and octyl **8** derivatives and on-going work will establish the orientations of our molecules relative to the interface plane. Work is in progress to take our findings here—at the pure 'solvent–solvent' interface—and localise similar molecules at ITIES, control their orientation by electric field, and study different electrochromic effects, be it in optical adsorption or SHG signal with applied potential, in order to create the first example of a light-driven molecular machine acting at ITIES.

Experimental section

General procedures

All preparations were carried out using standard Schlenk techniques. All solvents were distilled over standard drying agents under nitrogen directly before use, and all reactions were carried out under an atmosphere of nitrogen.

All NMR spectra were recorded using a Delta upgrade on JEOL EX270 400 and 500 MHz Bruker spectrometers. Chemical shifts are reported in δ (ppm) using $CDCl_3$ (^{1}H δ 7.26 ppm), acetone-d_6 (^{1}H δ 2.05 ppm), D_2O (^{1}H δ 4.75 ppm) as the reference solvents. Mass spectra were recorded using positive FAB methods for the methyl iodide salts and EI for the rest of the complexes, on a micromass Autospec Q spectrometer. Infrared spectra were recorded as KBr disks on a Perkin Elmer Spectrum RX FTIR spectrometer. Microanalyses were carried out by Mr S. Boyer at SACS (Scientific Analysis and Consultancy Services) at the University of North London. All other chemicals were purchased from the Aldrich Chemical Co.

Fluorescence imaging was performed using a confocal laser scanning microscope (Leica TCS SP2), coupled to a CW argon-ion laser (488 nm). The fluorescence emission of **6** and **8** from the thin layer of solution placed between the glass coverslips was spectrally dispersed using a prism and detected using a PM tube. Water immersion 63× objective (NA = 1.2) was used in all measurements.

Synthesis of 1

4-Iodopyridine (205 mg, 1.0 mmol), 4-(diphenylamino)phenyl boronic acid (318 mg, 1.1 mmol) and dimethoxyethane (DME) (12 ml) were placed in a Schlenk tube under an atmosphere of nitrogen. Sodium carbonate (315 mg, 3 mmol) was dissolved in a minimum volume of water. The catalyst, $Pd(PPh_3)_4$ (46 mg, 0.022 equiv.), was added to the DME solution of the reactants, followed immediately by addition of the sodium carbonate solution. After stirring at room temperature for 1 h, the temperature was increased to 90 °C for 16 h. The solvent was removed under reduced pressure, the resultant oily residue dissolved in ethyl acetate–chloroform (2 : 1) and subjected to column chromatography on SiO_2. The second major, yellow fraction was collected. Evaporation of solvent gave the required product **1** as a colourless solid (240 mg, 75% isolated yield).

^{1}H NMR (400 MHz) δ ($CDCl_3$): 8.62 (d, 2H, J = 6.0 Hz, C_5H_4N), 7.52 (d, 2H, J = 11.0 Hz, C_6H_4), 7.47 (d, 2H, J = 6.0 Hz, C_5H_4N), 7.32–7.27(m, 4H, *ortho*-C_6H_5), 7.16–7.06 (m, 8H, *meta*-, *para*-C_6H_5, C_6H_4); ^{13}C NMR (100 MHz) 149.17, 148.92, 147.68, 147.16, 129.37, 127.58, 124.93, 123.57, 122.80, 120.80; MS (EI 70 eV) m/z = 322 [M^+], 244 [$M^+ - C_5H_4N$], 78 [C_5H_4N]; HRMS: m/z = 322.1463 (calc. for $C_{23}H_{18}N_2$: 322.1469); anal. calc. for $C_{23}H_{18}N_2$: C, 85.68; H, 5.63; N, 8.69. Found C, 85.59; H, 5.68; N, 8.71%.

Synthesis of 2

4-(Diphenylamino)phenyl boronic acid (318 mg, 1.1 mmol), 3-iodo-pyridine (205 mg, 1.0 mmol) and DME (12 ml) were placed in a Schlenk tube under an atmosphere of nitrogen. $Pd(PPh_3)_4$ (46 mg) was added to the solution, along with sodium carbonate (315 mg, 3 mmol) dissolved in a minimum volume of water. After stirring at room temperature for 1 h the mixture was heated for 16 h at 70 °C. The solvent was evaporated under reduced pressure and the crude product was subjected to column chromatography on silica gel (eluent: *n*-hexane–$CHCl_3$ 1 : 1). The first main fraction contained the pure product, which after evaporation gave red-orange crystals of **2** (yield 293 mg, 80%).

^{1}H NMR (400 MHz) δ ($CDCl_3$): 8.84 (d, 1H, J = 1.6 Hz, C_5H_4N), 8.54 (dd, 1H, J = 4.8 Hz, 1.6 Hz, C_5H_4N), 7.84 (d of t, 1H, J = 8.4 Hz, 1.6 Hz, C_5H_4N), 7.45 (d, 2H, J = 8.3 Hz, C_6H_4), 7.33 (dt, 1H, J = 8.4 Hz, 4.8 Hz, C_5H_4N), 7.30–7.26 (m, 4H, *ortho*-C_6H_5), 7.17–7.03 (m, 8H, *meta*-, *para*-C_6H_5, C_6H_4); ^{13}C NMR (100 MHz) 148.00, 147.92, 147.43, 136.13, 133.68, 131.25, 129.34, 127.74, 124.68, 123.55, 123.48, 123.27; MS (EI 70 eV) m/z = 322[M^+]; anal. calc. for $C_{23}H_{18}N_2$: C, 85.68; H, 5.63; N, 8.69. Found C, 85.61; H, 5.57; N, 8.59%.

Synthesis of 3

A similar procedure to the synthesis of **2** was followed except that 1-iodo-4-nitrobenzene (249.0 mg, 1.0 mmol) was utilised. **3** was isolated as red-orange crystals (yield 293 mg, 80%).

^{1}H NMR (400 MHz) δ ($CDCl_3$) 8.26 (d, 2H, J = 8.8 Hz, $C_6H_4NO_2$), 7.69 (d, 2H, J = 8.8 Hz, $C_6H_4NO_2$), 7.50 (d, 2H, J = 8.4 Hz, C_6H_4), 7.32–7.27 (m, 4H, *ortho*-C_6H_5), 7.16–7.06 (m, 8H, *meta*-, *para*-C_6H_5, C_6H_4); ^{13}C NMR (100 MHz) 148.86, 147.18, 147.04, 146.49, 131.56, 129.45, 128.05, 126.85, 125.05, 124.17, 123.70, 122.82; MS (EI 70 eV) m/z = 366 [M^+], 320 [$M^+ - NO_2$]; HRMS: m/z = 366.1368 (calc. for $C_{24}H_{18}N_2O_2$: 366.1368); anal. calc. for $C_{24}H_{18}N_2O_2$: C, 78.67; H, 4.95; N, 7.65. Found C, 78.60; H, 4.89; N, 7.61%.

Synthesis of 4

A similar procedure to the synthesis of **2** was followed except that 4-iodobenzaldehyde (232.0 mg, 1.0 mmol) was utilised. **4** was isolated as red-orange crystals (yield 297 mg, 82%).

^{1}H NMR (270 MHz) δ ($CDCl_3$) 10.02 (s, 1H, CHO), 7.92 (d, 2H, J = 8.1 Hz, C_7H_5O), 7.72 (d, 2H, J = 8.1 Hz, C_7H_5O), 7.51 (d, 2H, J = 8.6 Hz, C_6H_4), 7.32–7.25 (m, 4H, *ortho*-C_6H_5), 7.15–7.04 (m, 8H, *meta*-, *para*-C_6H_5, C_6H_4); IR (KBr, cm^{-1}): 1691; MS (EI 70 eV) m/z = 349 [M^+]; HRMS m/z = 349.1464 (calc. for $C_{25}H_{19}NO$: 349.1466); anal. calc. for $C_{25}H_{19}NO$: C, 85.93; H, 5.48; N, 4.01. Found C, 85.87; H, 5.64; N, 3.95%.

Synthesis of 5

A similar procedure to the synthesis of **2** was followed except that 4-iodo-acetophenone (246.0 mg, 1.0 mmol) was utilised. **5** was isolated as red-orange crystals (yield 308 mg, 85%).

^{1}H NMR (400 MHz) δ ($CDCl_3$) 8.01 (d, 2H, J = 8.0 Hz, C_8H_7O), 7.66 (d, 2H, J = 8.0 Hz, C_8H_7O), 7.52 (d, 2H, J = 8.4 Hz, C_6H_4), 7.31–7.26 (m, 4H, *ortho*-C_6H_5), 7.16–7.05 (m, 8H, *meta*-, *para*-C_6H_5, C_6H_4), 2.63 (s, 3H, CH_3); ^{13}C NMR (100 MHz) 197.56, 148.13, 147.36, 145.13, 135.28, 133.07, 129.33, 128.91, 127.86, 126.42, 124.73, 123.31, 123.23, 26.55; IR (KBr, cm^{-1}): 1678; MS (EI 70 eV) m/z = 363 [M^+]; HRMS m/z = 363.1617 (calc. for $C_{26}H_{21}NO$: 363.1623); anal. calc. for $C_{26}H_{21}NO$: C, 85.92; H, 5.82; N, 3.85. Found C, 85.93; H, 5.86; N, 3.79%.

Synthesis of 6

1 (100 mg, 0.30 mmol) was dissolved in methyl iodide (7 ml). The solution was stirred for 30 min at room temperature and the product precipitated as a yellow solid. After filtration and washing with Et_2O, the crude product was recrystallised from CH_2Cl_2–*n*-pentane giving yellow needles of **6** (132 mg, 92% yield).

^{1}H NMR (400 MHz) δ ($CDCl_3$) 9.07 (d, 2H, J = 6.0 Hz, $C_5H_4N^+$), 8.08 (d, 2H, J = 6.0 Hz, $C_5H_4N^+$), 7.65 (d, 2H, J = 8.4 Hz, C_6H_4), 7.34–7.31 (m, 4H, *ortho*-C_6H_5), 7.18–7.13 (m, 6H, *meta*-, *para*-C_6H_5), 7.03 (d, 2H, J = 8.4 Hz, C_6H_4), 4.53 (s, 3H, CH_3); ^{13}C NMR (100 MHz) 154.85, 145.75, 144.79, 129.76, 129.02, 126.19, 125.29, 123.87, 122.66, 120.27, 47.94; MS FAB (+ve, nba) m/z = 337 [M^+]; anal. calc. for $C_{24}H_{21}N_2I$: C, 62.08; H, 4.56; N, 6.03. Found C, 61.98; H, 4.51; N, 5.94%.

Synthesis of 7

1 (100 mg, 0.30 mmol) was dissolved in methyl iodide (7 ml). The solution was stirred for 30 min at room temperature and the product precipitated as a yellow solid. After filtration and washing with Et_2O, the crude product was recrystallised from CH_2Cl_2–*n*-pentane giving yellow needles of **7** (120 mg, 83% yield).

^{1}H NMR (400 MHz) δ ($CDCl_3$) 9.32 (s, 1H, C_5H_4N), 9.03 (d, 1H, J = 5.6 Hz, C_5H_4N), 8.47 (d, 1H, J = 8.42 Hz, C_5H_4N), 8.03 (dd, 1H, J = 5.6 Hz, 4.0 Hz, C_5H_4N), 7.68 (d, 2H, J = 8.9 Hz, C_6H_4), 7.33–7.25 (m, 4H, *ortho*-C_6H_5), 7.15–7.07 (m, 8H, *meta*-, *para*-C_6H_5, C_6H_4), 4.74 (s, 3H, CH_3); MS FAB (+ve, nba) m/z = 337 [M^+]; anal. calc. for $C_{24}H_{21}N_2I$: C, 62.08; H, 4.56; N, 6.03. Found C, 61.99; H, 4.47; N, 5.93%

Synthesis of 8

A mixture of **1** (100 mg, 0.30 mmol) and 1-iodooctane (7 ml) was heated for 16 h at 70 °C. The product precipitated as a yellow solid, and after filtration under reduced pressure and washing with Et_2O, it was recrystallised from CH_2Cl_2–*n*-pentane giving yellow needles of **8** (140 mg, 80% yield).

^{1}H NMR (400 MHz) δ ($CDCl_3$) 9.11 (d, 2H, J = 7.2 Hz, $C_5H_4N^+$), 8.10 (d, 2H, J = 7.2 Hz, $C_5H_4N^+$), 7.66 (d, 2H, J = 8.8 Hz, C_6H_4), 7.37–7.33 (m, 4H, *ortho*-C_6H_5), 7.18–7.15 (m, 6H, *meta*-, *para*-C_6H_5), 7.05 (d, 2H, J = 8.8 Hz, C_6H_4), 4.75 (t, 2H, J = 7.6 Hz, $N^+CH_2(CH_2)_6CH_3$), 2.04–1.96 (m, $N^+CH_2(CH_2)_6CH_3$), 1.41–1.16 (m, $N^+CH_2(CH_2)_6CH_3$), 0.84 (t, 3H, J = 6.8 Hz, $N^+CH_2(CH_2)_6CH_3$); ^{13}C NMR (100 MHz) 154.98, 145.75, 143.94, 129.81, 129.04, 126.27, 125.39, 123.82, 122.76, 120. 24, 60.63, 31.62, 28.98, 28.96, 16.02, 22.53, 14.01; MS FAB (+ve, nba) m/z = 435 [M^+], 322 [$M^+ - C_8H_{17}$]; anal. calc. for $C_{31}H_{35}N_2I$: C, 66.19; H, 6.27; N, 4.98. Found C, 66.15; H, 6.26; N, 4.92%.

Synthesis of 9

To finely powdered **1** (200 mg, 0.60 mmol) concentrated HCl solution (40 ml) was added. The resulting suspension was sonicated and then stirred at room temperature for 30 min. Upon stirring colourless **1** was slowly dissolved to form a yellow solution. Removal of the solvent *in vacuo* effected precipitation of a yellow solid which was filtered off and dried under vacuum overnight. The crude product was recrystallised from CH_2Cl_2–*n*-pentane giving yellow needles of **9** (345 mg); anal. calc. for $C_{23}H_{19}N_2Cl{\cdot}2CH_2Cl_2{\cdot}H_2O$: C, 54.92; H, 4.61; N, 5.12. Found C, 55.12; H, 4.91; N, 5.13%.

Synthesis of 10

To a solution of **1** (100 mg, 0.30 mmol) in CH_2Cl_2 (2 ml), 3-chloroperoxo benzoic acid (105 mg, 0.60 mmol) was added at 0 °C. The resultant mixture was stirred at room temperature for 1 h and then the reaction was quenched by addition of aqueous $NaHCO_3$ solution. The organic layer was separated and evaporated to dryness, and the crude product was subjected to column chromatography on silica (ethyl acetate–chloroform 80 : 8). The product was eluted as the final yellow fraction and after evaporation of solvent afforded an oily yellow solid **10**.

^{1}H NMR (400 MHz) δ ($CDCl_3$) 8.20 (d, 2H, J = 7.2 Hz, C_5H_4NO), 7.46–7.43 (m, 4H, C_5H_4NO, C_6H_4), 7.31–7.27 (m, 4H, *ortho*-C_6H_5), 7.14–7.07 (m, 8H, *meta*-, *para*-C_6H_5, C_6H_4); ^{13}C NMR (100 MHz) 149.02, 147.03, 139.24, 138.28, 129.49, 128.74, 127.04, 125.13, 123.86, 122.72, 122.69; MS (EI 70 eV) m/z = 338 [M^+], 322 [M^+ – O]; HRMS m/z = 338.1417 (calc. for $C_{23}H_{18}N_2O$ 338.1419); anal. calc. for $C_{23}H_{18}N_2O$: C, 81.63; H, 5.36; N, 8.28. Found C, 81.58; H, 5.27; N, 8.19%.

Crystal data for **3**: $C_{24}H_{18}N_2O_2$, M = 366.40, monoclinic, $P2_1/c$ (no. 14), a = 13.3702(3), b = 15.0329(3), c = 9.6952(2) Å, β = 104.763(2)°, V = 1884.34(7) Å^3, Z = 4, D_c = 1.292 g cm^{-3}, μ(Mo-Kα) = 0.083 mm^{-1}, T = 173 K, orange blocky needles, Oxford Diffraction Xcalibur 3 diffractometer; 6348 independent measured reflections, F^2 refinement, R_1 = 0.045, wR_2 = 0.131, 4504 independent observed absorption-corrected reflections [$|F_o| > 4\sigma(|F_o|)$, $2\theta_{max}$ = 65°], 253 parameters. CCDC 696198.

Crystal data for **6**: $(C_{24}H_{21}N_2)$(I), M = 464.33, monoclinic, $P2_1/n$ (no. 14), a = 5.69284(14), b = 40.9581(10), c = 9.1109(2) Å, β = 101.802(2)°, V = 2079.46(9) Å^3, Z = 4, D_c = 1.483 g cm^{-3}, μ(Mo-Kα) = 1.550 mm^{-1}, T = 173 K, yellow needles, Oxford Diffraction Xcalibur 3 diffractometer; 4216 independent measured reflections, F^2 refinement, R_1 = 0.044, wR_2 = 0.113, 3113 independent observed absorption-corrected reflections [$|F_o| > 4\sigma(|F_o|)$, $2\theta_{max}$ = 54°], 384 parameters. CCDC 696199.

Crystal data for **9**: $(C_{23}H_{19}N_2)$(Cl)·0.5H_2O·0.25CH_2Cl_2, M = 389.09, triclinic, $P\bar{1}$ (no. 2), a = 9.0670(17), b = 10.852(2), c = 21.500(4) Å, α = 100.431(15), β = 90.436(15), γ = 103.375(16)°, V = 2021.4(7) Å^3, Z = 4 (2 independent molecules), D_c = 1.278 g cm^{-3}, μ(Cu-Kα) = 2.367 mm^{-1}, T = 173 K, yellow plates, Oxford Diffraction Xcalibur PX Ultra diffractometer; 7479 independent measured reflections, F^2 refinement, R_1 = 0.062, wR_2 = 0.159, 3741 independent observed absorption-corrected reflections [$|F_o| > 4\sigma(|F_o|)$, $2\theta_{max}$ = 142°], 525 parameters. CCDC 696200.

Acknowledgements

MKK is thankful to the EPSRC Life Sciences Interface programme for a personal fellowship. We would like to thank Dr Klaus Suhling for the use of the confocal fluorescence microscope, and the EPSRC for funding this work *via* the 'Adventurous Chemistry' programme.

References

1 I. Benjamin, *Chem. Rev.*, 2006, **106**, 1212.
2 W. H. Steel and A. W. Walker, *Nature*, 2003, **424**, 296.
3 K. B. Eisenthal and E. A. McArthur, *J. Am. Chem. Soc.*, 2006, **128**, 1068.
4 Z. Samec and T. Kakiuchi, *Advanced Electrochemistry and Electrochemical Science*, ed. H. Gerischer and C. W. Tobias, VCH, Weinheim, 1995, p. 297.
5 H. H. Girault and D. H. Schiffrin, *Electroanalytical Chemistry*, ed. A. J. Bard, Dekker, New York, 1989, vol. 15, p. 1; H. H. Girault, *Modern Aspects of Electrochemistry*, ed. J. O'M. Bockris *et al.*, Plenum, New York, 1993, vol. 25, p. 1.
6 C. M. Starks, C. L. Liotia and M. Halpern, *Phase Transfer Catalysis*, Chapman and Hall, New York, 1994.
7 A. G. Volkov, D. W. Deamer, D. I. Tanelian and V. S. Markin, *Liquid Interfaces in Chemistry and Biology*, Wiley, New York, 1998.
8 B. Su, J.-P. Abid, D. J. Fermin, H. H. Girault, H. Hoffmannova, P. Krtil P and Z. Samec, *J. Am. Chem. Soc.*, 2004, **126**, 915.
9 B. J. Coe, J. A. Harris, I. Asselberghs, K. Wostyn, K. Clays, A. Persoons, B. S. Brunschwig, S. J. Coles, T. Gelbricht, M. E. Light, M. B. Hursthouse and K. Nakatani, *Adv. Funct. Mater.*, 2003, **13**, 347.
10 V. Balzani and F. Scandola, *Supramolecular Photochemistry*, Ellis Horwood, New York, 1991, p. 427.
11 A. A. Kornyshev, M. Kuimova, A. M. Kuznetsov, J. Ulstrup and M. Urbakh, *J. Phys.: Condens. Matter*, 2007, **19**, 375111.
12 J. Dobkowski, J. Wojcik, W. Kozminski, R. Kolos, J. Waluk and J. Michl, *J. Am. Chem. Soc.*, 2002, **11**, 2406.
13 H. Yangi, N. Matsuoka, M. Kondo, M. Nagawa and Y. Taniguchi, *Langmuir*, 2001, **17**, 5491.
14 T. Verbiest, D. M. Burland, M. C. Jurich, V. Y. Lee, R. D. Miller and W. Volksen, *Science*, 1995, **268**, 1604.
15 M. Yano, Y. Ishida, K. Aoyama, M. Tatsumi, K. Sato, D. Shiomi, A. Ichimura and T. Takui, *Synth. Met.*, 2003, **137**, 1275.
16 S. Tanaka, T. Iso and Y. Doke, *Chem. Commun.*, 1997, 2064.
17 H. Tanaka, S. Tokito, Y. Taga and A. Okada, *Chem. Commun.*, 1996, 2175.
18 G. Barnes and I. Gentle, *Interfacial Science An Introduction*, Oxford University Press Inc., New York, 2005, p. 264.

